Quaternary International 503 (2019) 136–145

Contents lists available at ScienceDirect

Quaternary International

journal homepage: www.elsevier.com/locate/quaint

Automatic identification of the lake area at Qinghai–Tibetan Plateau using remote sensing images

Zhaofei Liu*, Zhijun Yao, Rui Wang**

Institute of Geographic Sciences and Natural Resources Research, Chinese Academy of Sciences, 100101, Beijing, China

ARTICLE INFO

Keywords:
Automatic interpretation
Area error analyses
Sub-pixel classification
Lake area change
Landsat 8
Tibetan plateau

ABSTRACT

The lake area of the Qinghai-Tibetan Plateau (QTP) was identified using an automatic waterbody interpretation method. The spectral reflectance of water is much lower than that of other land-surface materials in remote sensing images. The method made use of this characteristic, and divided the lake area into pure water pixels and mixed pixels. In total, 4051 field-collected ground control points of the boundaries of the 17 lakes were used to calibrate and validate the method. The lake area changes from the 1980s to 2015 were also analyzed. It can deal with the mismatch between the grid image boundaries and vector real lake boundaries. Results indicate that it is necessary to consider this mismatch when identifying waterbodies based on remote sensing images, especially in the case of waterbodies with an irregular shape. The method can distinguish waterbodies from wetlands and glaciers, and the interpretation accuracy was improved. In 2015, 1177 lakes with an area larger than 1 km^2 were recorded; the total lake area of the QTP was 43873.6 km^2. In general, the QTP lakes have expanded during the past several decades. The lake area has increased by 18.3% from the 1980s to 2015. This indicates expansion in the Northern Tibetan Plateau and shrinkage in the southern region of the QTP. The changes of precipitation were the main reasons for lake area changes on the QTP. However, the increased glacier melt runoff played a dominant role in the upper regions of the Yalungzangbo and Yellow rivers. The method proposed herein can be easily applied to other studies to monitor waterbodies based on remote sensing images, especially in the case of large waterbodies.

1. Introduction

Lakes are key components of the Earth's surface system; they are points at which the atmosphere, geosphere, hydrosphere, and biosphere meet. Lakes are sensitive to global and regional environmental changes. Most of the lakes in China are greatly affected by human activities. However, the lakes of the Qinghai–Tibetan Plateau (QTP) still reflect their natural status and climatic conditions. The lakes of the QTP are therefore sensitive indicators for climate change. The monitoring of lake area changes is essential with respect to the regional environment and climate change issues; it benefits the research on the local cryosphere, ecosystem changes, energy, and hydrological cycle. The investigation of QTP lake data is considerably challenging because of the harsh natural conditions. The lake area of a few lakes has been analyzed based on field-stationed observations. Remote sensing provides an effective method to monitor lake changes due to the increased availability of remote sensing platforms with adequate spatial and temporal resolutions, near global coverage, and low financial costs (Song et al., 2014; Biskop et al., 2016).

Climate change characterized by rapidly rising temperatures and changing precipitation and evapotranspiration has substantially impacted the water storage of the inland lakes on the QTP during the past decades. In particular, the rapidly rising temperature accelerated the glacier retreat and permafrost thawing, which is considered to be closely associated with enhanced lake expansions (Yao et al., 2007; Song et al., 2014). Recently, literature focusing on alpine lake changes and their response to climate change has been rapidly increasing. In most of the studies, the lake area on the QTP was extracted by manual visual interpretation (Bian et al., 2009; Ma et al., 2011; Wan et al., 2014; Lei et al., 2014; Yan and Zheng, 2015). A main drawback of the manual visual method is that the interpretation results contain a large amount of artificial effects. In other words, different researchers obtain different interpretation results.

Several automatic interpretation methods can be used to identify lakes based on remote sensing images. The normalized difference water index (NDWI) uses multispectral bands to enhance the water features

* Corresponding author.
** Corresponding author.
E-mail addresses: zfliu@igsnrr.ac.cn (Z. Liu), wangr@igsnrr.ac.cn (R. Wang).

https://doi.org/10.1016/j.quaint.2018.10.023
Received 5 March 2018; Received in revised form 19 August 2018; Accepted 19 October 2018
Available online 21 October 2018

and has been widely applied to identify waterbodies in various regions. It also eliminates several noise components such as mountain shadows and light cloud covers. The method mainly comprises three indexes, NDWIs–$NDWI_{Green/NIR}$ (McFeeters, 1996), $NDWI_{NIR/MIR}$ (Gao, 1996), and $NDWI_{Green/MIR}$ (Xu, 2006), which are calculated by [(Green − NIR)/(Green + NIR)], [(NIR − MIR)/(NIR + MIR)], and [(Green − MIR)/(Green + MIR)], respectively. Liu et al. (2016) evaluated these methods based on field data and found that the $NDWI_{Green/NIR}$ identifies the waterbodies best.

The threshold selection is a key step in identifying waterbodies based on a single band or NDWI images. McFeeters (1996) suggested that the threshold of $NDWI_{Green/NIR}$ can be set to zero. Liu et al. (2016) calibrated the threshold of $NDWI_{Green/NIR}$ using field data and set it to −0.05. This can lead to the overestimation or underestimation of water areas when using an arbitrary empirically selected threshold because the threshold values vary with regions. Threshold adjustment in individual situations can achieve a more accurate delineation of waterbodies (Ji et al., 2009). Frequency histograms have been used for threshold selection to extract waterbodies from images (Ryu et al., 2002; Lacaux et al., 2007). However, this is time-consuming, especially in the case of large study areas with many lakes. In addition, not all of these methods can distinguish waterbodies from wetlands and glaciers.

Although there has been much improvement with respect to the spatial and temporal resolution of remote sensing images, accuracy assessment is still necessary for the interpretation of images (Gao and Liu, 2001). The calculation of uncertainties from multi-satellite images was developed by William et al. (1997) and is widely used in glacier mapping based on images (Hall et al., 2003; Silverio and Jaquet, 2005). However, it is not suitable for the single-image accuracy assessment. The accuracy assessment for single images requires referenced data such as GPS data (Frezzotti et al., 1998). However, there is always a mismatch between the grid data boundary and vector boundary (Liu and Yao, 2016); any boundary grid always comprises a fractional area of waterbodies, which can be estimated by dividing the images into subpixel components. Several methods can be used for the separation of the images into subpixels such as the fuzzy, maximum likelihood, Bayesian, and linear spectral mixture (LSM) classifications. The LSM method differs from many other methods; it links the image spectra to the laboratory or field spectral reflectance of materials and hence is a physical-based image processing method (Weng and Lu, 2008).

The object of this study is to identify the QTP lake area and lake area changes from 1980s to 2015 based on remote sensing images. An automatic interpretation method is developed to identify waterbodies using images. Based on the fact that the spectral reflectance of water is much lower than that of other land-surface materials, it is relative easier to identify pure water pixels in an image. Therefore, the lake area was divided into pure water pixels and mixed pixels in images. Field-observed data of lake boundaries over the QTP were used for the calibration and validation of the method. The mismatch between the grid data and vector lake boundaries is also be considered using subpixel analyses. The automatic interpretation method can be easily applied to other studies to identify waterbodies based on images, especially for large study areas.

2. Materials and methods

2.1. Study area

The QTP is the highest and most extensive plateau on Earth at an average altitude of more than 4000 m (Fig. 1). Its area is about 250×10^4 km^2. More than 1000 lakes larger than 1 km^2 are located on the plateau. Also, the statistics from 2005 to 2006 showed that the number of lakes that have surface areas greater than 10 km^2, 100 km^2, 500 km^2, and 1000 km^2 were 389, 81,13 and 3, respectively. The total area of the QTP lakes accounts for ~51.4% of the total lake area in China (Ma et al., 2011). This region is characterized by rather complex topography and climate patterns. These alpine QTP lakes show a strong spatial and temporal variability and different responses to climate change because of the diverse climatic and topographical patterns. The QTP and surrounding area contain the largest number of glaciers outside of the Polar Regions (Yao et al., 2012). These glaciers are experiencing extensive shrinkage (Yao et al., 2007), which affects the local hydrological processes.

2.2. Dataset

2.2.1. Field data

A total of 4051 ground control points (GCP) of the boundaries of the 17 lakes were collected during 2013 and 2016 (Fig. 1); remote sensing images were acquired on the same day. The coordinates of the control points were recorded using a Magellan Triton 400 handheld global positioning system (GPS) device. Its built-in signal augmentation reception provided an accuracy of 3 m.

The field GCPs are located at the boundaries of 17 lakes on the QTP. The lake area, water depth, turbidity, and quality of these lakes vary. The lake area ranges from 1.7 to 413.6 km^2. There are three and seven lakes with areas lower than 10 km^2 and larger than 100 km^2, respectively. The water depth adjacent to the lake boundary varies from 0.2 to 2.5 m. The water turbidity adjacent to the lake boundary ranges from 0.8 to 329.2 NTU. The total dissolved solid (TDS) concentration of the water is lower than 1 g/L in some lakes, while it is larger than 60 g/L in other lakes. The water salinity is lower than 1 g/L in some lakes, while it is larger than 70 g/L in other lakes. The lake boundaries adjacent to the field GCPs were therefore representative for different kinds of lake boundaries of the QTP.

2.2.2. Remote sensing data

Landsat 8 OLI images were used in this study. The OLI sensor provides improved signal-to-noise (SN) radiometric performance quantized over a 12-bit dynamic range. This translates into 4096 potential grey levels in an image compared with only 256 grey levels produced by eight-bit instruments. The improved SN performance enables the better characterization of the conditions of the land cover. The multispectral Landsat 8 OLI images were obtained from http://glovis.usgs.gov/. Seven images of 17 lakes were acquired using field GCPs during the field period. In total, 119 images that covered the QTP were selected to identify the lake area. These images were mainly recorded from May to October 2015; a few images were also obtained from May to October 2014 or 2016. The seasonal changes of the lake area were not included in this study. Because it is too hard to collect all images in the same period for this large area.

The correction and calibration of the images is fundamental for all applications to achieve a satisfactory representation of the Earth's surface. The raw pixel values of the images (digital numbers, DN) were converted to true measures of reflective power (spectral radiance). The radiance image data were then atmospherically corrected to obtain the spectral reflectance images. Details of the image processing can be found in the Landsat 8 Science Data Users' Handbook (http://landsat7.usgs.gov/Landsat8_Using_Product.php).

2.3. Methods

2.3.1. The normalized difference water index

The $NDWI_{Green/NIR}$ used in this study was calculated from the multispectral Landsat 8 OLI images. “Green” and “NIR” (near-infrared) represent Landsat 8 OLI bands 3 and 5, respectively. Thus, $NDWI_{Green/NIR}$ was referred to as $NDWI_{35}$ in this study. Note that the wavelengths of these two Landsat 8 bands were in the ranges of the corresponding Landsat 7 bands but showed slight differences. The $NDWI_{35}$ of the Landsat 8 OLI images was calculated as follows:

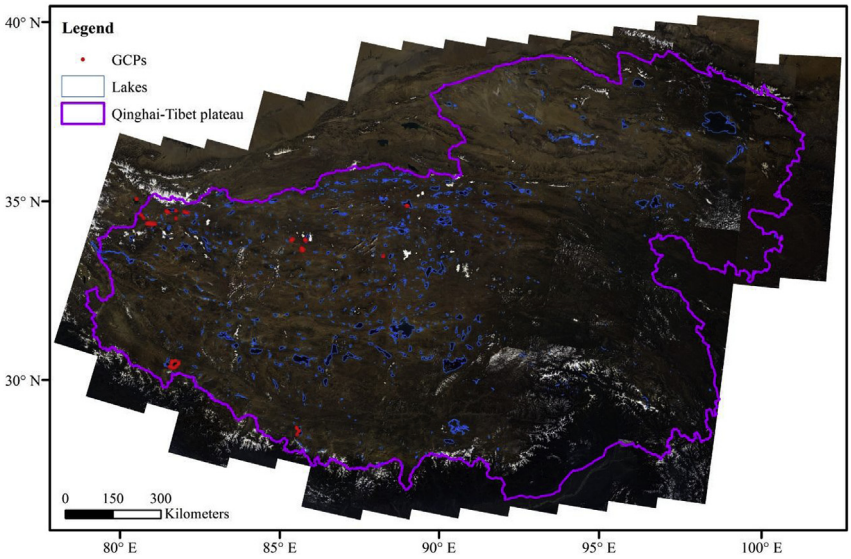

Fig. 1. Location of the QTP lakes and ground control points (The base map is from Landsat 8 OLI images data).

$$NDWI_{35} = \frac{band3 - band5}{band3 + band5} \quad (1)$$

The $NDWI_{35}$ was calculated from the spectral reflectance image.

2.3.2. Automatic interpretation method to identify waterbodies

The $NDWI_{35}$ can enhance the water features in a remote sensing image, especially that of pure water pixels. It was found that the $NDWI_{35}$ values of pure water pixels adjacent to the GCPs are usually larger than that of other land features including glaciers and wetlands. Therefore, it is easy to identify pure water pixels from a $NDWI_{35}$ image. The automatic interpretation method for the identification of waterbodies proposed in this study is the following:

1. Identification of the optimized threshold for the pure water pixels. Based on the GCPs and corresponding $NDWI_{35}$ images, the threshold for the pure water pixels is selected using the constraint functions,

$$N_m = \sum_{i=1}^{n} GCP_i \quad (2)$$

and

$$GCP_i = \begin{cases} 1, & if \ \ V_{threshold} < V_{water}, \ and \ \ V_{GCP} < V_{threshold} \\ 0, & else \end{cases} \quad (3)$$

where N_m is the number of correct GCPs located along the boundary pixels of classified waterbodies when a trial threshold is used; GCP_i is the ith GCP; n is the number of GCPs used; V_{GCP} is the pixel value of the GCP; V_{water} is the pixel value of pure water, which is adjacent to the GCP; and $V_{threshold}$ is the threshold value computed from the minimum value of the GCP pixels to their maximum value. Its interval is 0.01.

2. Identification of the pure water pixel polygons. The pure water pixels are identified as the constraint function, where the pixel value is larger or equal to the optimized threshold. The polygons of the pure water pixels are then generated and the area of the pure water pixels (A_{pw}) is calculated.
3. The polygons of the pure water pixels are outside-buffered by 30 m. The buffered pixels correspond to the mixed pixels of water and land. In fact, the lake shorelines are included in the mixed pixels. The polygons of the mixed pixels are also outside-buffered by 30 m; the buffered pixels correspond to pure land pixels.
4. The LSM method is applied to calculate the water area of the waterbodies in any mixed pixel. The calculation is as follows,

$$f = \frac{R_m - R_l}{R_w - R_l} \quad (4)$$

where f is the fraction of the waterbodies and R_m, R_l, and R_w is the reflectance of the mixed, land, and waterbody pixels, respectively. The water area of the mixed pixels (A_{mw}) is obtained by multiplying the area of mixed pixels with the fraction.

5. The accurate lake area is the sum of A_{pw} and A_{mw}.

One advantage of this automatic interpretation method is that it is easy to identify the pure water pixels in a NDWI image because the pixel values of pure water are generally larger than that of other land types. This method was described as the Pure Water & Mixed Boundary (PWMB) method.

3. Results

3.1. Evaluation of the PWMB method

Based on the 4051 GCPs, the optimized threshold for the pure water pixel was identified as 0.30. Then, the lake boundaries extracted by the PWMB method were evaluated by GCPs. The number of correct GCPs for this method was 4016, which accounts for 99.1% of the total GCPs. The threshold of 0, which was usually used for the waterbody interpretation based on remote sensing image, was also evaluated by GCPs. The results showed that the correct GCPs only accounts for 71.3% of the total GCPs. Fig. 2 shows mixed pixel boundaries the Guozha Co lake extracted by the PWMB and the threshold 0, respectively. It could be seen from the figure that the PWMB method was able to estimate the lake boundary, with almost all GCPs was located in the mixed pixel boundary. But the threshold 0 method lost its ability to estimate the lake boundary, especially for mixed pixels affect by clouds or wetlands. Fig. 3 shows the pixel values of the mixed (GCPs), pure water, and pure land adjacent to the GCPs in the $NDWI_{35}$ images.

3.2. The QTP lake area in 2015

The polygons of pure water, mixed, and pure land pixels were identified based on the optimized threshold for the pure water pixels. The fractional area of the waterbodies in any mixed pixel was calculated using the LSM method. The results showed that there were 1177 lakes with areas larger than 1 km^2 in 2015; the total QTP lake area was

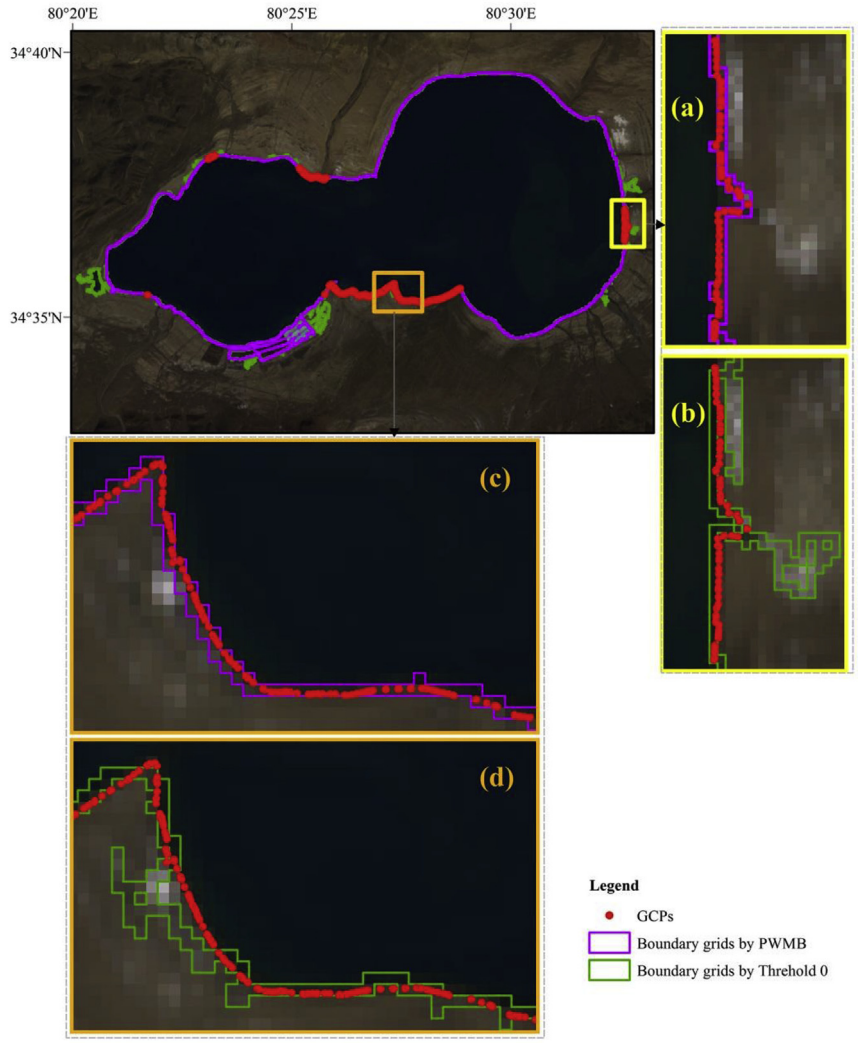

Fig. 2. Comparison of the PWMB method and the threshold 0 by ground control points (GCPs) in the Guozha Co lake.

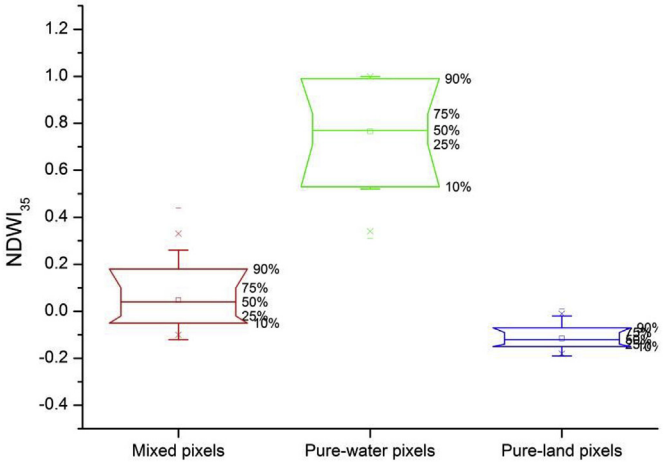

Fig. 3. Pixel values of mixed (ground control points), pure-water and pure-land adjacent to ground control points in $NDWI_{35}$ images.

43873.6 km^2. It should be noted that multiple lakes that combined were counted as single lake in this study (Fig. 8). The classification of the QTP lakes based on the lake area is shown in Table 1. The largest three lakes were the Qinghai Lake, Selin Co (also called Siling Co), and Nam Co with a lake area of 4514.5 km^2, 2397.1 km^2, and 2019.6 km^2,

Table 1
Results of QTP lakes area in 2015.

Classification (km^2)	Number	Area (km^2)	
		Average	Total
> 1000	4	2499.8	9999.1
> 500 and < 1000	8	673.6	5398.1
> 100 and < 500	78	205.5	16025.7
> 50 and < 100	72	68.8	4952.9
> 10 and < 50	225	22.3	5010.5
> 1 and < 10	790	3.2	2496.3

respectively. Because of the lake expansion, the water surfaces of four lakes including Tu Co (also called Dolsodong Co), Kongnam Co, Mitijiangzhanmu Co, and Maqiao Co were combined and the total lake area was 1067.9 km^2. In addition, the area of Zhari Namco is 998.2 km^2, which is close to 1000 km^2. Ninety lakes were larger than 100 km^2; the area of these lakes accounted for up to 71.6% of the QTP lake area. The lake area of the lakes larger than 10 km^2 accounted for 94.3% of the QTP lake area. This indicates that the big lakes played a major role on the QTP, which is consistent with results of Zhang et al. (2014).

The mismatch (area differences) between the grid image boundaries and vector real lake boundaries of 346 QTP lakes from Chinese Lake Records (Wang and Dou, 1998) was analyzed. These lakes include all QTP lakes of the 1980s with areas larger than 10 km^2. Fig. 4 shows the

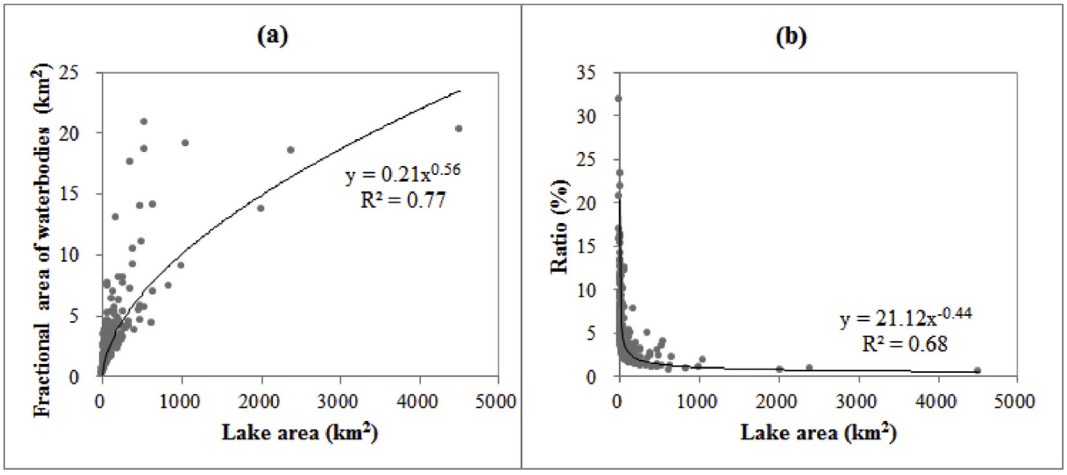

Fig. 4. Scatter plots for (a) lake area and fractional water area in mixed boundary pixels, (b) lake area and ratio of fractional water area to lake area.

scatter plots for the (a) lake and fractional water areas of the mixed boundary pixels and the (b) lake areas and ratio of the fractional water area to lake area. The results show that the fractional water area of the mixed boundary pixels of the 346 lakes was larger than 800 km^2. The area accounted for more than 2.0% of the total lake area. In general, the fractional water area of a lake is proportional to the lake perimeter. The largest fractional area of 20.9 km^2 (3.9% of the total lake area) was determined for the Yamzhog Yum Co Lake (also called Yamdrok Lake). The irregular, narrow and long lake shape of the lake caused the great lake perimeter. Similar large lakes (area > 500 km^2) include the Xijir Ulan, Ulan Ul, and Dogai Coring lakes. The ratio of the fractional water area to the total lake area is generally large for small lakes (area < 50 km^2). For example, the largest ratio was 31.8% for the Dongcaoalong Lake, with a lake area of only 2.0 km^2. The ratio of the Yigong Co Lake reached 23.3%; the lake area was 14.6 km^2. The ratio was also larger than 5% in eight medium lakes (50 km^2 < area < 500 km^2) including the Bangong Lake (356.5 km^2 area), Chaka Salt Lake, and Xitaijinair Lake (ratio > 12%). In addition, the mean value of the fractional water area was 17.9 km^2 for lake areas larger than 1000 km^2; it was 10.9 km^2 for lake areas larger than 500 km^2 and lower than 1000 km^2.

The area of the 346 lakes identified by the PWMB method proposed in this study was also compared with that extracted by the threshold of 0. The results showed that the total area of the 346 lakes was 39572.2 km^2 when the PWMB method was used. The lake area was overestimated by 2.9%, when the threshold of 0 was used. The area of 27 lakes was overestimated by > 10 km^2 when the threshold of 0 was applied. The greatest overestimation was 134.9 km^2 for the Zhabuye Salt Lake. In addition, the overestimation of the Charhan and Chaka salt lakes exceeded 55 km^2. The area overestimation was greater than 10% for 49 lakes. Fig. 5 shows the comparison of the lake boundaries identified by the PWMB method and the threshold 0. The overestimated water area identified by the threshold of 0 is mainly located in the wetlands at lake boundaries. This was verified by field GCPs, which are located in the wetlands at lake boundaries. The results of the GCPs showed that the $NDWI_{35}$ values in wetlands are usually larger than 0 but lower than 0.3. Several lakes showed little difference including the Kusai, Qixiang Co, Jiesa Co, Taiyang, Gemang Co, and Dajia Co lakes. These lakes are located in the intermountain basins. Each lake has a regular, smooth, and steep lakeshore.

3.3. Changes of the QTP lakes

The area changes of the QTP lakes from the 1980s and 2005–2006 to 2015 are shown in Fig. 6. The data of the 1980s were obtained from the Chinese Lake Records, while that from 2005 to 2006 were obtained from the results of Wan et al. (2014). The actual lake area data in the Chinese Lake Records were recorded from the 1960s–1980s. For convenient description, 1980s was used instead of that period in this study. The salt lakes recorded in the 1980s were not included. In general, the QTP lakes have experienced an expansion during the past several decades. From the 1980s to 2015, the QTP lake area of lakes larger than 1 km^2 and 10 km^2 increased by 6820.8 km^2 and 6413.9 km^2, respectively.

In this section, 312 of the 346 lakes were analyzed, except for the salt lakes. The results showed that the total lake area increased by 4749.3 km^2 from the 1980s to 2015. Lake expansion was observed for 230 lakes; the area increased by 5467.7 km^2. Seventy-nine lakes shrank; the area decreased by 718.4 km^2. Three of the shrinkage lakes disappeared or became little waterbodies with areas lower than 1 km^2 (Fig. 9). In addition, the lake area of 17 lakes decreased below 10 km^2 in 2015.

The spatial distribution of the area changes for each lake is shown in Fig. 7. In general, the QTP lakes display expansion on the North Tibetan Plateau, while they show shrinkage in the southern region of the QTP. Twenty-four lakes with an area increment larger than 50 km^2 were detected; they are mainly located in the central and northern regions of the QTP. The largest area increment of 736.1 km^2 was determined for the Selin Co Lake. It increased from 1662.8 km^2 in the 1980s to 2389.9 km^2 in 2015. The Duogecuorenqiang Co Lake exhibits the second largest area increment of 191.4 km^2. It increased from 207.5 km^2 to 398.9 km^2. Ten lakes showed an area increment larger than 100 km^2, for example, large lakes (area > 500 km^2), such as the Qinghai, the Selin Co, and Ulan Ul lakes, or small lakes such as the Yan Lake (area of 20 km^2 in the 1980s). The greatest area decrement of 102.2 km^2 was determined for the Zhuonai Lake. The Yamzhog Yum Co Lake also displayed an area decrement of 84.7 km^2. However, all other lake area decrements were lower than 40 km^2; 59 lakes showed decrements < 10 km^2. Generally, this indicated that lake shrinkage is not as notable as lake expansion on the QTP.

Sixty-five lakes showed relative changes > 40%; they were mainly located in the central and northern regions of the QTP. Most of them were small lakes (area < 50 km^2). However, one large and 18 medium-sized lakes were also included. The large lake is the Selin Co Lake, which increased by 44.3% from the 1980s to 2015. Sixteen lakes exhibited relative changes larger than 100%. The greatest relative change was 665.7%, observed for the Yan Lake. Twelve lakes had relative changes lower than −40%, mainly including small lakes located in the southern region of the QTP. The lowest relative change was −89.6%, observed for the Cuojiangqin Lake, which is a barrier lake recorded in the Chinese Lake Records. In addition, seventy-seven lakes showed little changes (−5%–5%). In other words, these lakes were relatively stable

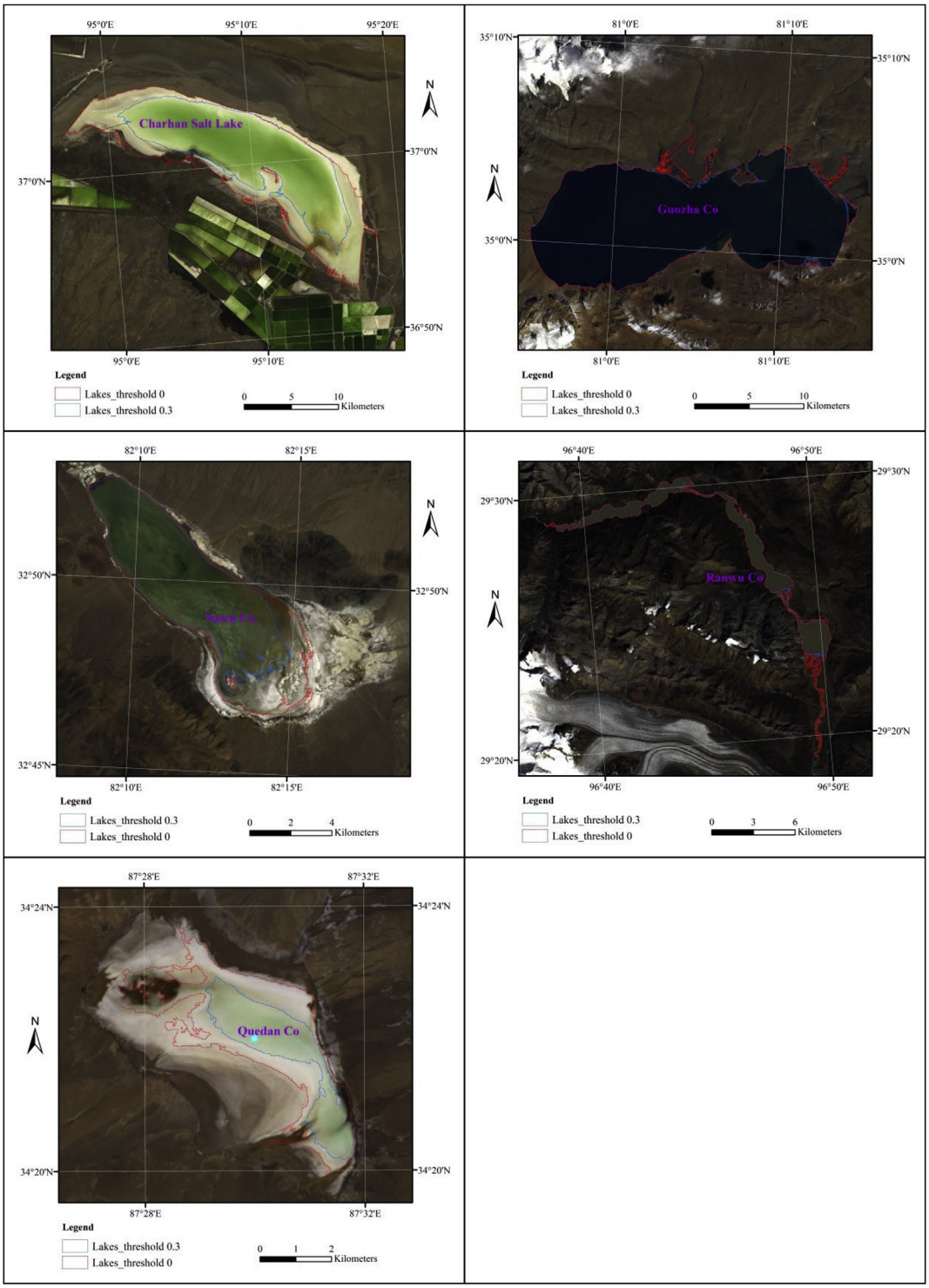

Fig. 5. Several lake boundaries identified by the method proposed in this study and the threshold 0.

from the 1980s to 2015. Spatially, these lakes were mainly located between expansion and shrinkage lakes (Fig. 7). Although they showed notable area expansion, they were relatively stable. For example, the Nam Co and the Qinghai lakes showed a relative change of 3.0% and 4.1%, respectively.

Because of the lake expansion, 31 adjacent lakes recorded in the Chinese Lake Records were combined to 14 lakes in 2015 (Fig. 8). The relative change of each lake was greater than 15%. These lakes were located in the central and northern regions of the QTP, where the lake area is characterized by significant expansion trends. The 31 separate lakes recorded in the Chinese Lake Records were counted as 14 lakes in this study.

In addition to the 346 lakes recorded in the Chinese Lake Records, 60 new lakes with areas larger than 10 km^2 were found in 2015 (Fig. 9) including five artificial reservoirs such as the Longyangxia and Pangduo reservoirs with water areas of 355.4 km^2 and 36.3 km^2, respectively. In contrast, the area of the other three reservoirs was smaller than 15 km^2. The new lakes are mainly located on the Northern Tibetan Plateau that showed lake expansion trends. Only seven 7 lakes with areas larger than 20 km^2 were observed. Although the lakes in southern TP

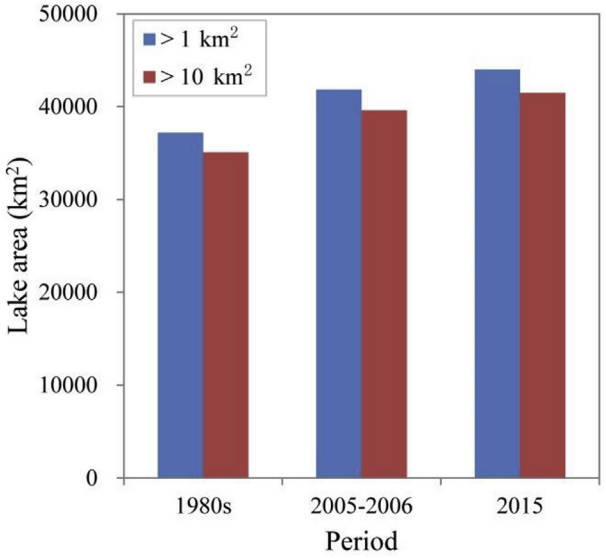

Fig. 6. Area changes of the QTP lakes larger than 1 km^2 (Data of 1980s was obtained from results of Wang and Dou (1998), while that of 2005–2006 was obtained from results of Wan et al. (2014).).

generally show a shrinking trend, this lake (largest one at uppper Yaungzangbo) expanded that may be caused by increased glacier melts. The area expansion of the lakes in the upper region of the Yellow River, such as that of the Zhaling and Eling lakes, is similar. The area expansion of the Zhaling Lake was caused by more glacier melt runoff in the upper region of the Yellow River, while that of the Eling Lake might be due to both more glacier melt runoff and the impact of an artificial reservoir (Wen et al., 2015). The lake area of the Yuedao and Tuzhong lakes, which are located on the North Tibetan Plateau, also increased to a size > 30 km^2. In addition, three lakes recorded in the Chinese Lake Records disappeared (or became small waterbodies with areas < 1 km^2) including the Dingjie Co, Longria Co, and Gansenquan lakes (see Fig. 9).

4. Discussion

Remote sensing is a useful technique for water monitoring. Although it is easier to identify waterbodies than other land-cover types from images, traditional automatic waterbody interpretation methods still have some problems. In this study, an automatic waterbody interpretation method based on the extraction of pure water pixels was proposed. The method solved two problems: 1) The mismatch (area differences) between the grid image and vector real lake boundaries was evaluated; and 2) The lake area could not be distinguished from wetlands and glaciers using the traditional method.

The mismatch between the grid data and vector boundaries always existed in remote sensing images but was rarely studied. A solution based on the subpixel classification was used to analyze these area differences in this study. The water area of mixed pixels was calculated with the LSM method based on GCPs. The area differences of the 346 lakes showed that the water area of the mixed pixels accounts for more than 2% of total lake area and is proportional to the lake perimeter. In general, the ratio of the water area to lake area is large for small lakes; it was > 20%. In the case of medium-sized lakes such as the Bangong Lake with an area of 356.5 km^2, it was larger than 5%. In general, the water area of the mixed pixels in lake boundaries cannot be neglected when identifying lake areas based on remote sensing images, especially for lakes with irregular shapes. In other words, area error analyses for the grid image and vector real boundaries need to be considered when identifying waterbodies based on images, especially in the case of waterbodies with irregular shapes.

The 4051 GCPs of the boundaries of 17 lakes collected in the field were used to calibrate the optimized threshold for the pure water pixels. The results showed that the optimized threshold for the pure water pixels of the $NDWI_{35}$ images was 0.3. The $NDWI_{35}$ values for mixed pixels of water and land, wetlands, and glaciers were generally larger than 0. Therefore, wetlands and glaciers cannot be distinguished from waterbodies using the traditional method with a threshold of 0 because waterbodies include mixed pixels. The traditional method can be used for lakes with regular, smooth, and steep lakeshores. However, it tends to overestimate the lake area, especially in the case of lakes with irregular shapes or wetlands located in lakeshore regions. The wetlands and glaciers could be distinguished from the waterbodies and the interpretation accuracy could be improved using the optimized threshold for the pure water pixels because the $NDWI_{35}$ values of wetlands and glaciers were generally lower than 0.3.

In gneral, the QTP lakes have shown an expansion during the past several decades. From the 1980s to 2015, the QTP lake area increased by 18.3%. It showed expansion on the northern Tibetan Plateau, while it displayed shrinkage trends in the southern region of the QTP. This is consistence with results of Lei et al. (2014) and Fang et al. (2016). A new lake was found to have an area larger than 1000 km^2 due to lake expansion; several adjacent lakes have joined water surfaces. It was also observed that the large Anglaren Co Lake with an area of 512.7 in the 1980s decreased to a medium lake size (area < 500 km^2). Sixty new lakes with areas > 10 km^2 were detected in 2015; they are due to climate change or artificial reasons.

During the past several decades, the precipitation and air temperature increased, while the potential evapotranspiration decreased on the QTP (Yang et al., 2014). These climate changes had positive effects on the water balance. The increased precipitation and decreased potential evapotranspiration generated more runoff to supply the lake water. In addition, more glacier melt runoff induced by increasing air temperature also supplied lake water. The spatial distribution of precipitation changes shows an increase on the Northern Tibetan Plateau, while it displays a decrease in the southern region of the QTP (Yang et al., 2014), consistent with lake area changes. The decreasing potential evapotranspiration in the southern region of the QTP indicated that the evapotranspiration is not a dominant factor affecting on the lake area changes in this region. Overall, the changes of precipitation are responsibly for the lake area changes on the QTP. This is consistence with other results (Lei et al., 2014; Zhou et al., 2015, 2016; Zhang et al., 2017; Dai et al., 2018). For example, Zhou et al. (2015, 2016) used a distributed hydrological model and found that lake water storage changes were largely depended on precipitation. Zhang et al. (2017) found increased precipitation contributed the majority of water supply (74%) for the lake increase by the water balance method. Lei et al. (2014) found the significant water surplus is mainly attributed to increased regional precipitation based on regression analyses. In the upper regions of the Yalungzangbo and Yellow rivers, the precipitation and potential evapotranspiration showed a decrease and increase, respectively. But lake area showed slightly expansion in these regions. It might be explained by the increased glacier melt runoff, because of acceleration of glacier retreat in these regions (Bibi et al., 2018).

The Zhuonai Lake burst on September 14, 2011, due to the increasing precipitation. The outburst water ran into the Yan Lake, inducing the greatest relative lake change (665.7%) on the QTP. The precipitation on the QTP is still increasing. In addition to the increasing glacier melt runoff, this might cause the outburst of lakes and disasters with respect to the local ecology system and human activities.

In addition to these natural reasons, the impact of human activities on lakes is mainly reflected by artificial reservoirs and the development of salt lakes. Five reservoirs with areas larger than 10 km^2 were detected. The total water area was 433.1 km^2. Salt lakes were mainly located in the Qinghai Province.

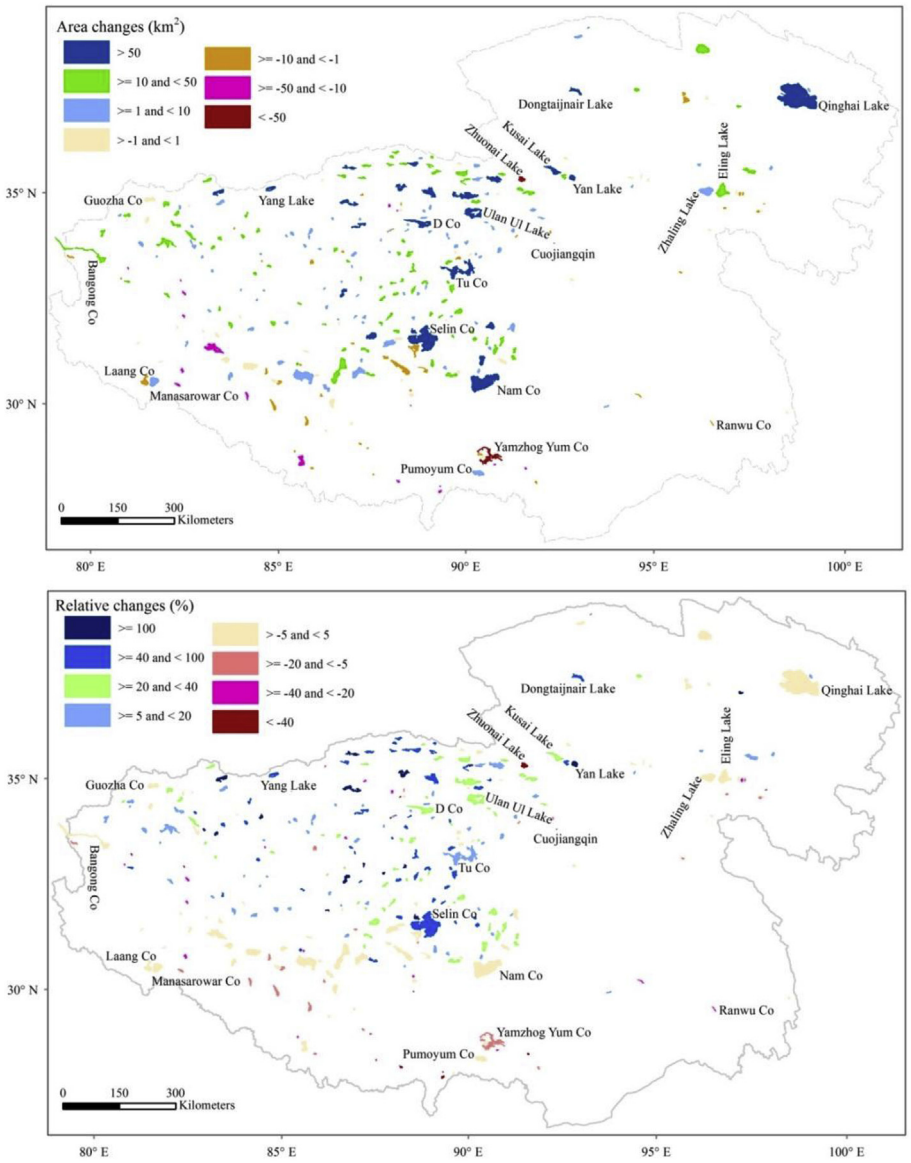

Fig. 7. Area changes of the 346 QTP lakes from the 1980s to 2015 ("D Co" is Duogecuorenqiang Co).

5. Conclusions

The lake area of the QTP was identified using an automatic waterbody interpretation method. The spectral reflectance of water is much lower than that of other land-surface materials in remote sensing images. The method made use of this characteristic, and divided the lake area into pure water pixels and mixed pixels. In total, 4051 field-collected GCPs of the boundaries of 17 lakes were used to calibrate and validate the method. The lake area changes from the 1980s to 2015 were analyzed. Several conclusions were drawn:

1) The pure water pixel-based automatic waterbody interpretation method was proposed in this study. The optimized threshold for the pure water pixels of the $NDWI_{35}$ images is 0.3. Wetlands and glaciers could be distinguished from waterbodies and the interpretation accuracy was improved. The method is robust and can easily be applied to other studies to monitor waterbodies in remote sensing images, especially for waterbodies with large areas.
2) In the identification of waterbodies from remote sensing images, the mismatch between the grid images and vector boundaries was evaluated. This mismatch was larger than 800 km^2. The ratio of the mismatch to the lake area was larger than 10% and 20% for some medium and small lakes, respectively. It concluded that area error analyses with respect to this mismatch need to be considered when identifying waterbodies in remote sensing images, in particular in the case of waterbodies with irregular shapes.
3) In total, 1177 lakes with areas larger than 1 km^2 were detected on the QTP; the total lake area was 43873.6 km^2. In general, the QTP lakes have shown an expansion during the past decades. The total lake area increased by 18.3% from the 1980s to 2015. Because of the lake expansion, 31 adjacent lakes recorded in the Chinese Lake Records combined to 14 lakes. Sixty new lakes with areas larger than 10 km^2 were detected in 2015, including five artificial reservoirs.
4) The results imply expansion on the North Tibetan Plateau and shrinkage in the southern region of the QTP. The precipitation changes are mainly responsible for the lake area changes on the QTP. However, the increased glacier melt runoff played a dominant role in the upper regions of the Yalungzangbo and Yellow rivers.

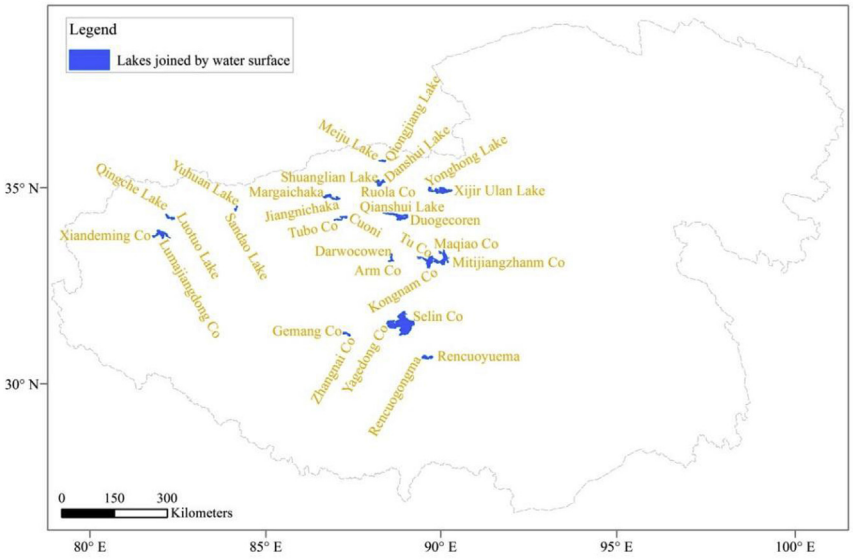

Fig. 8. The adjacent lakes which were recorded in the 1980s, but had joined by water surface in 2015.

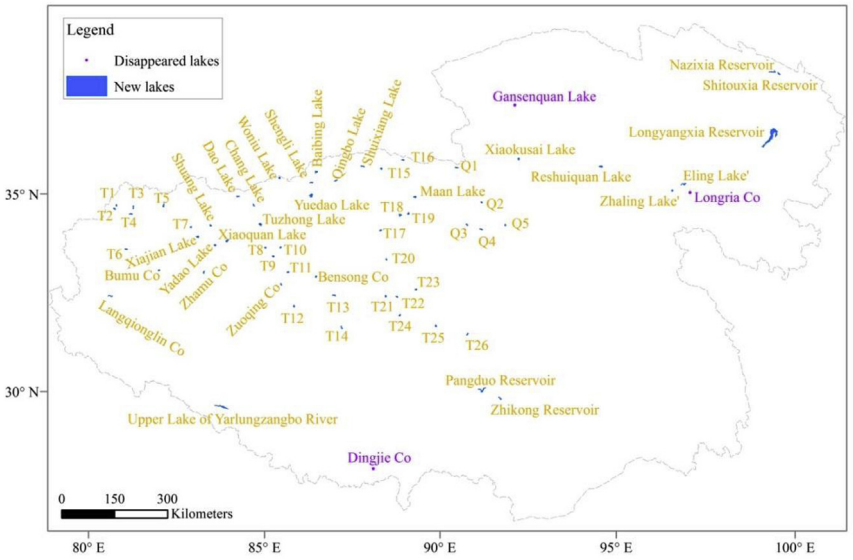

Fig. 9. New lakes larger than 10 km^2 in 2015 and disappeared lakes recorded in the 1980s over the QTP ("T" and "Q" represent lakes without names located in Tibet Autonomous Region and Qinghai Province respectively).

Acknowledgement

This study was supported and funded by the National Key Research and Development Program of China (2016YFC0401306) and National Natural Science Foundation of China (41571027, 41561144012 and 4161101254).

References

Bian, B., Bianba, C., Li, L., Wang, W., Zhaxi, Y., 2009. The response of lake change to climate fluctuation in north Qinghai-Tibet Plateauau in last 30 years. J. Geogr. Sci. 19, 131–142.

Bibi, S., Wang, L., Li, X.P., Zhou, J., Chen, D.L., Yao, T.D., 2018. Climatic and associated cryospheric, biospheric, and hydrological changes on the Tibetan Plateau: a review. Int. J. Climatol. 38, 1–17.

Biskop, S., Maussion, F., Krause, P., Fink, M., 2016. Differences in the water-balance components of four lakes in the southern–central Tibetan Plateau. Hydrol. Earth Syst. Sci. 20, 209–225.

Dai, Y., Wang, L., Yao, T., Li, X., Zhu, L., Zhang, X., 2018. Observed and simulated lake effect precipitation over the Tibetan Plateau: an initial study at Nam Co Lake. J. Geophys. Res. D: Atmos. 123, 6746–6759.

Fang, Y., Cheng, W., Zhang, Y., Wang, N., Zhao, S., Zhou, C., Chen, X., Bao, A., 2016. Changes in inland lakes on the Tibetan Plateau over the past 40 years. J. Geogr. Sci. 26, 415–438.

Frezzotti, M., Capra, A., Vittuari, L., 1998. Comparison between glacier ice velocities inferred from GPS and sequential satellite images. Ann. Glaciol. 27, 54–60.

Gao, B.C., 1996. NDWI-A normalized difference water index for remote sensing of vegetation liquid water from space. Remote Sens. Environ. 58, 257–266.

Gao, J., Liu, Y.S., 2001. Applications of remote sensing, GIS and GPS in glaciology: a review. Prog. Phys. Geogr. 25, 520–540.

Hall, D.K., Bayr, K., Schfner, W., Bindschadler, R.A., Chien, Y.L., 2003. Consideration of the errors inherent in mapping historical glacier positions in Austria from ground and space (1893-2001). Remote Sens. Environ. 86, 566–577.

Ji, L., Zhang, L., Wylie, B., 2009. Analysis of dynamic thresholds for the normalized difference water index. Photogramm. Eng. Rem. Sens. 75, 1307–1317.

Lacaux, J.P., Tourre, Y.M., Vignolles, C., Ndione, J.A., Lafaye, M., 2007. Classification of ponds from high–spatial resolution remote sensing: application to Rift Valley Fever epidemics in Senegal. Remote Sens. Environ. 106, 66–74.

Lei, Y.B., Yang, K., Wang, B., Sheng, Y.W., Bird, B.W., Zhang, G.Q., Tian, L.D., 2014. Response of inland lake dynamics over the Tibetan Plateau to climate change. Climatic Change 125, 281–290.

Liu, Z., Yao, Z., Wang, R., 2016. Assessing methods of identifying open water–bodies using Landsat 8 OLI image. Environ. Earth Sci. 75, 1–13.

Liu, Z., Yao, Z., 2016. Area errors between grid images boundaries and vector actual boundaries identifying water–bodies from remote sensing image. Communications in Computer and Information Science 569, 682–692.

Ma, R.H., Yang, G.S., Duan, H.T., Jiang, J.H., Wang, S.M., Feng, X.Z., Li, A.N., Kong, F.X.,

Xue, B., Wu, J.L., Li, S.J., 2011. China's lakes at present: number, area and spatial distribution. Sci. China Earth Sci. 54, 283–289. https://doi.org/10.1007/s11430–010–4052–6.
McFeeters, S.K., 1996. The use of the Normalized Difference Water Index (NDWI) in the delineation of open water features. Int. J. Rem. Sens. 17, 1425–1432.
Ryu, J.H., Won, J.S., Min, K.D., 2002. Waterline extraction from Landsat TM data in a tidal flat: a case study in Gomso Bay, Korea. Remote Sens. Environ. 83, 442–456.
Silverio, W., Jaquet, J.M., 2005. Glacial cover mapping (1987-1996) of the Cordillera Blanca (Peru) using satellite image. Remote Sens. Environ. 95, 342–350.
Song, C., Huang, B., Ke, L., Richards, K.S., 2014. Remote sensing of alpine lake water environment changes on the Tibetan Plateau and surroundings: a review. ISPRS J. Photogrammetry Remote Sens. 92, 26–37.
Wan, W., Xiao, P.F., Feng, X.Z., Li, H., Ma, R.H., Duan, H.T., Zhao, L.M., 2014. Monitoring lake changes of Qinghai–Tibetan Plateau over the past 30 years using satellite remote sensing data. Chin. Sci. Bull. 59, 1021–1035.
Wang, S.M., Dou, H.S., 1998. Chinese Lake Records. Science Press, Beijing.
Wen, L., Lv, S., Li, Z., Zhao, L., Nagabhatla, N., 2015. Impacts of the two biggest lakes on local temperature and precipitation in the Yellow River source region of the Tibetan Plateau. Adv. Meteorol. 248031.
Weng, Q.H., Lu, D.S., 2008. A sub-pixel analysis of urbanization effect on land surface temperature and its interplay with impervious surface and vegetation coverage in Indianapolis, United States. Int. J. Appl. Earth Obs. Geoinf. 10, 68–83.
Williams, R.S.J., Hall, D.K., Sigurdsson, O., Chien, J.Y.L., 1997. Comparison of satellite–derived with ground–based measurements of the fluctuations of the margins of Vatnajfkull, Iceland, 1973–92. Ann. Glaciol. 24, 72–80.
Xu, H., 2006. Modification of normalised difference water index (NDWI) to enhance open water features in remotely sensed image. Int. J. Rem. Sens. 27, 3025–3033.
Yan, L.J., Zheng, M.P., 2015. The response of lake variations to climate change in the past forty years: a case study of the northeastern Tibetan Plateau and adjacent areas, China. Quat. Int. 371, 31–48.
Yang, K., Wu, H., Qin, J., Lin, C., Tang, W., Chen, Y., 2014. Recent climate changes over the Tibetan Plateau and their impacts on energy and water cycle: a review. Global Planet. Change 112, 79–91.
Yao, T., Thompson, L., Yang, W., Yu, W., Gao, Y., Guo, X., Yang, X., Duan, K., Zhao, H., Xu, B., Pu, J., Lu, A., Xiang, Y., Kattel, D.B., Joswiak, D., 2012. Different glacier status with atmospheric circulations in Tibetan Plateau and surroundings. Nat. Clim. Change 2, 663–667.
Yao, T., Pu, J., Lu, A., Wang, Y., Yu, W., 2007. Recent glacial retreat and its impact on hydrological processes on the Tibetan Plateau, China, and surrounding regions. Arctic Antarct. Alpine Res. 39, 642–650.
Zhang, G.Q., Yao, T.D., Shum, C.K., Yi, S., Yang, K., Xie, H., Feng, W., Bolch, T., Wang, L., Behrangi, A., Zhang, H., Wang, W., Xiang, Y., Yu, J., 2017. Lake volume and groundwater storage variations in Tibetan Plateau's endorheic basin. Geophys. Res. Lett. 44, 5550–5560.
Zhang, G.Q., Yao, T.D., Xie, H.J., Zhang, K.X., Zhu, F.J., 2014. Lakes' state and abundance across the Tibetan Plateau. Chin. Sci. Bull. 59, 3010–3021.
Zhou, J., Wang, L., Zhang, Y., Guo, Y., He, D., 2016. Spatiotemporal variations of actual evapotranspiration over the Lake Selin Co and surrounding small lakes (Tibetan Plateau) during 2003–2012. Sci. China Earth Sci. 59, 2441–2453.
Zhou, J., Wang, L., Zhang, Y., Guo, Y., Li, X., Liu, W., 2015. Exploring the water storage changes in the largest lake (Selin Co) over the Tibetan Plateau during 2003–2012 from a basin-wide hydrological modeling. Water Resour. Res. 51, 8060–8086.